Journal of Biomechanics 91 (2019) 7–13

Contents lists available at ScienceDirect

Journal of Biomechanics

journal homepage: www.elsevier.com/locate/jbiomech
www.JBiomech.com

A computational model for prediction of clot platelet content in flow-diverted intracranial aneurysms

Ali Sarrami-Foroushani [a], Toni Lassila [a], Seyed Mostafa Hejazi [b], Sanjoy Nagaraja [c], Andrew Bacon [d], Alejandro F. Frangi [a,e,*]

[a] Centre for Computational Imaging and Simulation Technologies in Biomedicine (CISTIB), School of Computing, University of Leeds, Leeds, UK
[b] Department of Electronic and Electrical Engineering, The University of Sheffield, Sheffield, UK
[c] Sheffield Teaching Hospitals, Sheffield, UK
[d] Department of Neurosurgery, Royal Hallamshire Hospital, Sheffield, UK
[e] Biomedical Imaging Department, Leeds Institute for Cardiovascular and Metabolic Medicine (LICAMM), School of Medicine, University of Leeds, Leeds, UK

ARTICLE INFO

Article history:
Accepted 30 April 2019

Keywords:
Flow diverter
Intracranial aneurysms
Thrombosis
Computational fluid dynamics

ABSTRACT

Treatment of intracranial aneurysms with flow-diverting stents is a safe and minimally invasive technique. The goal is stable embolisation that facilitates stent endothelialisation, and elimination of the aneurysm. However, it is not fully understood why some aneurysms fail to develop a stable clot even with sufficient levels of flow reduction. Computational prediction of thrombus formation dynamics can help predict the post-operative response in such challenging cases. In this work, we propose a new model of thrombus formation and platelet dynamics inside intracranial aneurysms. Our novel contribution combines platelet activation and transport with fibrin generation, which is key to characterising stable and unstable thrombus. The model is based on two types of thrombus inside aneurysms: red thrombus (fibrin- and erythrocyte-rich) can be found in unstable clots, while white thrombus (fibrin- and platelet-rich) can be found in stable clots. The thrombus generation model is coupled to a CFD model and the flow-induced platelet index (FiPi) is defined as a quantitative measure of clot stability. Our model is validated against an in vitro phantom study of two flow-diverting stents with different sizing. We demonstrate that our model accurately predicts the lower thrombus stability in the oversized stent scenario. This opens possibilities for using computational simulations to improve endovascular treatment planning and reduce adverse events, such as delayed haemorrhage of flow-diverted aneurysms.

1. Introduction

Treatment of large and wide-necked intracranial aneurysms of the anterior circulation with flow-diverting stents is safe and effective (Becske et al., 2013; Byrne and Szikora, 2012; Fischer et al., 2012). However, post-treatment rupture after seemingly successful treatment, reported in almost 2% of cases (Byrne and Szikora, 2012; Kulcsár and Szikora, 2012), is associated with high risks of mortality and morbidity. There is a growing consensus that assessment of thrombus composition must successfully predict flow diverter (FD) performance (Chow et al., 2012; Fischer et al., 2012; Kulcsár et al., 2011; Kulcsár and Szikora, 2012; Kuzmik et al., 2013; Turowski et al., 2011; Xiang et al., 2014). Two types of thrombi have been identified from autopsy studies of aneurysms: white thrombus, rich in fibrin and platelets (Fischer et al., 2012; Turowski et al., 2011), and red thrombus. Red thrombus is characterised by: (i) less enmeshed platelets (Fischer et al., 2012; Turowski et al., 2011), (ii) not facilitating the formation of a neointimal layer (Kadirvel et al., 2014; Szikora et al., 2015), (iii) being prone to continuous fibrinolysis and renewal (Turowski et al., 2011; Undas and Ariëns, 2011; Weisel and Litvinov, 2008), and (iv) inducing autolytic activities in the wall resulting in weakening of the wall and ultimately rupture (Fischer et al., 2012; Kulcsár et al., 2011; Turowski et al., 2011). Non-organised red thrombi after flow diversion has been suggested as a potential predictor for post-treatment rupture (Chow et al., 2012; Kuzmik et al., 2013; Fischer et al., 2012; Kulcsár et al., 2011; Kulcsár and Szikora, 2012; Turowski et al., 2011).

While the mechanisms of FD-induced thrombosis are not well understood, there is a consensus that blood flow stasis induced by flow diversion is the dominant driver of the clot formation in intracranial aneurysms. The clots found in flow-diverted aneurysms are closer in structure to those clots formed under stagnant

* Corresponding author at: Centre for Computational Imaging and Simulation Technologies in Biomedicine (CISTIB), School of Computing, University of Leeds, Leeds, UK.
E-mail address: a.frangi@leeds.ac.uk (A.F. Frangi).

https://doi.org/10.1016/j.jbiomech.2019.04.045
0021-9290/

flow in venous thrombosis rather than those formed in high shear-induced arterial thrombosis (Kulcsár et al., 2011; Park et al., 2017; Tan and Lip, 2003; Wolberg et al., 2012). In flow stasis, secretion of tissue factor by endothelium (Bodnár et al., 2014), white blood cells (Bodnár et al., 2014), and hypoxic platelets (Bodnár et al., 2014; Versteeg et al., 2013); and, secretion of platelet activating factors by endothelium (de Sousa et al., 2015) and hypoxic red blood cells (Bodnár et al., 2014; Aida and Shimano, 2013; Shimano et al., 2010) are associated with fibrin generation and platelet activation, the two major components of clot formation. Regions with low shear flow and high residence time promote platelet activation and adhesion (de Sousa et al., 2015; Ouared et al., 2008), and stabilisation of platelet aggregates (Nesbitt et al., 2009). They also enhance platelet-fibrin and platelet-endothelium interactions (Ouared et al., 2008). It has been hypothesised that platelets can be activated in high-shear regions near the FD struts or because of blood contact with the FD wires (Heller et al., 2013; Taylor et al., 2017). Such effects are avoided by dual antiplatelet therapies (Heller et al., 2013; Tan and Lip, 2003; Taylor et al., 2017) or modification/coating of the wires (Girdhar et al., 2018, 2019; Martínez-Galdámez et al., 2017) to minimise the risk of thromboembolic events distal to the aneurysm (Heller et al., 2013; Tan and Lip, 2003; Taylor et al., 2017). Hence, despite a diverse set of initiation mechanisms, flow stasis can be the nexus between them all. In our proposed model we focus on flow stasis as the pathway to thrombus formation.

While extensive computational investigations have focused on modelling thrombosis in flow systems, few studies have simulated coupled haemodynamics and biochemistry in flow-diverted aneurysms (Ngoepe and Ventikos, 2016; Ou et al., 2017). Taking thrombin concentration as a surrogate for thrombosis, Ngoepe and Ventikos (2016) simulated clot growth in aneurysms after flow diversion, and an assumption was made that thrombin generation originated on the endothelial wall due to tissue damage. Ou et al. (2017) focused on stasis-induced expression on blood-borne tissue factor as the initiator and simulated fibrin generation inside the flow-diverted aneurysm. Although these studies presented promising results on simulation-based prediction of FD-induced thrombosis, they did not predict the platelet composition of the clot or its stability. Our model is the first to attempt computational thrombus stability analysis in realistic three-dimensional aneurysms after flow-diversion.

The objective of this study is to create a coupled flow and thrombosis model capable of predicting the stability of the clot that forms after flow diversion. A computational thrombosis model must consider estimation of the clot extent and stability in terms of composition of its structural components, i.e. fibrin and platelets. We consider FD-induced stasis as a surrogate for all the above mentioned thrombosis initiation mechanisms and simultaneously model thrombin and fibrin generation, and platelet activation and aggregation in stagnation regions. We validate our model against an in vitro experiment performed in Gester et al. (2016), in which thrombus formation was examined in an aneurysm phantom treated with FD's of different sizes.

2. Materials and methods

2.1. Model of thrombosis after flow diversion

Our model is based on bulk initiation and propagation of thrombosis due to flow stasis. Increased flow residence time, decreased flow velocity, decreased shear rate, and decreased vorticity have been used to characterise flow stasis in aneurysms (Cebral et al., 2014; Ouared et al., 2016; Rayz et al., 2010). When compared with thrombosed regions, velocity, vorticity, and shear rate were reported to be 2.8 times larger in non-thrombosed regions of elastase-induced aneurysms in animal models (Cebral et al., 2014). Based on a harmonic analysis of shear rate waves in ten aneurysms, de Sousa et al. (2015) determined 25 s^{-1} as the threshold for thrombosis. Rayz et al. (2010) showed that thrombus deposits in aneurysmal regions with a residence time greater than 18.22 ± 11 s. We therefore assumed thrombosis to initiate and progress in *prothrombotic* regions of the aneurysm after flow diversion, i.e., regions with time-averaged shear rate smaller than $SR_t = 25\ s^{-1}$ (de Sousa et al., 2015) and residence time greater than $RT_t = 5$ s (Rayz et al., 2010).

We considered four biochemically-coupled events that result in a clot of fibrin mesh and aggregated platelets: (i) *Thrombin generation* occurs by conversion of prothrombin to thrombin on the surface of resting and activated platelets, where the reaction kinetics are faster for activated platelets. Also considered is thrombin inhibition by its primary plasma inhibitor (anti-thrombin), in the absence of heparin catalysis. (ii) *Fibrin generation* occurs in the presence of thrombin, which converts fibrinogen to fibrin monomers. We did not consider further polymerisation of the fibrin monomers. (iii) *Platelet activation* occurs when resting platelets become activated by exposure to thrombin or other activated platelets. The latter mechanism was a surrogate for activation by agonists released from other activated platelets (Kuharsky and Fogelson, 2001). (iv) *Platelet aggregation* in the presence of fibrin takes place when platelets attached to the fibrin network aggregate to form bound platelets. Bound platelets were assumed to activate prothrombin and other resting platelets. Our model included five biochemical species: prothrombin (PT), thrombin (TH), antithrombin (AT), fibrinogen (FG), fibrin (FI). Three categories of platelets; resting platelets (RP), activated platelets (AP), and fibrin bound aggregated platelets (BP) were considered. A schematic representation of the biochemical species and reactions is given in Fig. 1. Mathematical description of our thrombosis model and the governing equations are provided in the Supplementary Material.

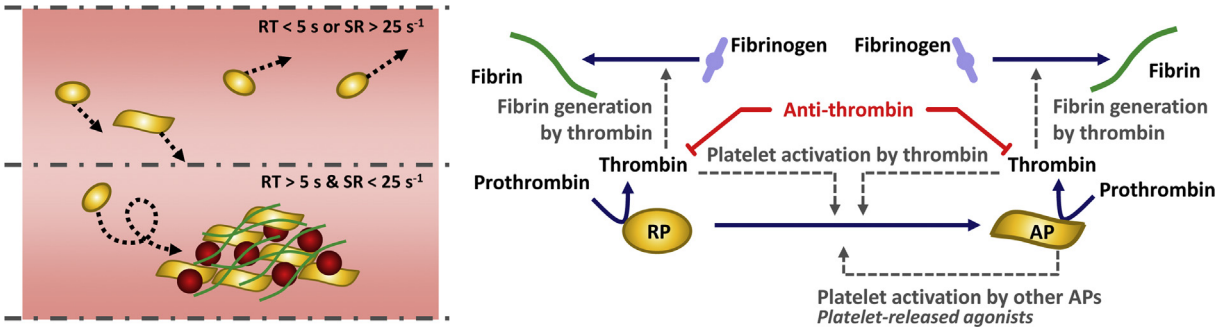

Fig. 1. Left panel: schematic representation of platelet transport to the clotting site. Right panel: schematic representation of the clotting reaction network modelled in this study.

2.2. Flow induced Platelet index (FiPi)

We defined the *flow induced platelet index* (FiPi) as the relative difference of the platelet concentration between a closed and an open system:

$$\mathcal{P} = \frac{C_{bp}^{open} - C_{bp}^{closed}}{C_{bp}^{closed}} = \frac{C_{bp}^{open}}{C_{rp,0} + C_{ap,0}} - 1. \quad (1)$$

In Eq. (1), $C_{rp,0}$ and $C_{ap,0}$ are initial concentrations of resting and activated platelets in the clot-free blood, respectively. FiPi quantifies the effect of blood flow on transport of platelets to and from the site of clot formation and consequently on the final platelet content of the formed clot. As shown in Fig. 2, in a closed system with no inflow or outflow, we assumed the concentration of bound platelets in a formed clot to be equal to the summation of the concentrations of resting and activated platelets at the initial state before any clot formed. However, in an open system, where blood can flow over and through the forming clot, the final concentration of bound platelets in the formed clot would differ from that in closed systems. In flow-diverted aneurysms, it has been hypothesised that the flow entering the sac brings platelets into contact with the forming clot and promotes formation of a higher platelet content clot (Xiang et al., 2014).

2.3. Computational model validation

Gester et al. (2016) evaluated intra-aneurysmal FD-induced thrombus formation. Two FD's of same type with two diameters were deployed in a silicone phantom of a simplified lateral aneurysm; one of the FD's had a diameter of 4.00 mm (FD-4.0) the other was oversized with a diameter of 4.50 mm (FD-4.5). The phantom aneurysm was spherical with an inner diameter of 6.4 mm and a neck width of 6.0 mm. The tubular parent vessel had an inner diameter of 4.2 mm with an angle of 120° at the aneurysm neck. Blood from the cervical artery of slaughter house pigs were circulated in the phantom model. Particle imaging velocimetry (PIV) and Doppler sonography were performed to monitor the flow inside aneurysm. The FD-induced intra-aneurysmal clots were qualitatively evaluated once the sonography signal no longer existed (i.e., 10–12 h after the experiments started). In the aneurysm treated with FD-4.0, a red cap-shaped clot was observed, mostly consisting of organised and platelet-rich clot formed with a growth direction opposite to the entering flow jet. In the aneurysm treated with the oversized stent, FD-4.5, a less platelet-rich clot filling almost the entire sac with no clear growth direction was observed with only a rigid (platelet-rich) region near the center of the aneurysm. We built computer models of the phantom experiments and compared computational simulations of the FD-induced thrombosis against in vitro observations reported in Gester et al. (2016). Details on the computer models and the numerical simulations are presented in the Supplementary Material.

3. Results

3.1. Aneurysmal haemodynamics before/after flow diversion

Table 1 shows pre- and post-treatment haemodynamic quantifications based on the flow simulations before the thrombosis was activated (the first set of simulations). Both FD configurations induced flow stasis in the aneurysm sac. Fig. 3 shows intra-aneurysmal haemodynamics along the aneurysm sagittal mid-plane before and immediately after FD deployment before any clot formed. To enable a qualitative comparison with the PIV measurements made in Gester et al. (2016), we ran pulsatile flow simulations, with no chemical reaction, and presented velocity contour plots at the peak systole. In Fig. 3, shear rate and residence time contour plots are taken from steady-state simulations and represent the time-averaged values.

Table 1
Haemodynamic quantifications before and immediately after FD placement, averaged over time and the sac. Values in parentheses indicate changes from the pre-FD quantity.

	Velocity [m/s]	Residence time [s]	Shear rate [s^{-1}]
Before FD placement	0.043	0.649	89.66
After FD placement			
FD-4.0	0.003(−93%)	7.504(+1,056%)	5.786(−94%)
FD-4.5	0.008(−81%)	1.947(+200%)	18.59(−79%)

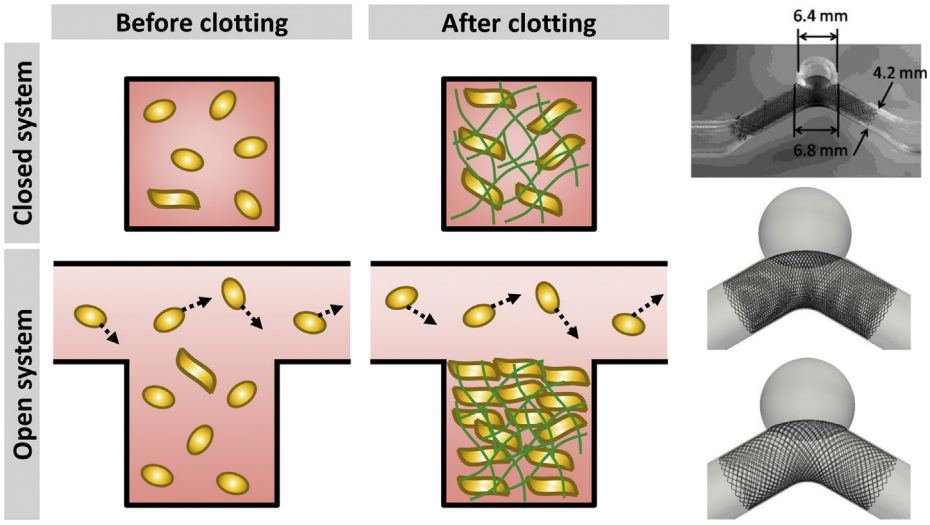

Fig. 2. The first two columns represent the concept of the flow-induced platelet index (FiPi). In a closed system, the platelet content of the clot is equal to the initial concentration of platelets in the container before clotting occurred. In an open system, more platelets are advected with the blood flow to the clotting site, where they can attach to the clot and increase the clot platelet content. The third column shows the phantom from Gester et al. (2016) (first row) and the computer models with FD-4.0 (second row) and FD-4.5 (third row).

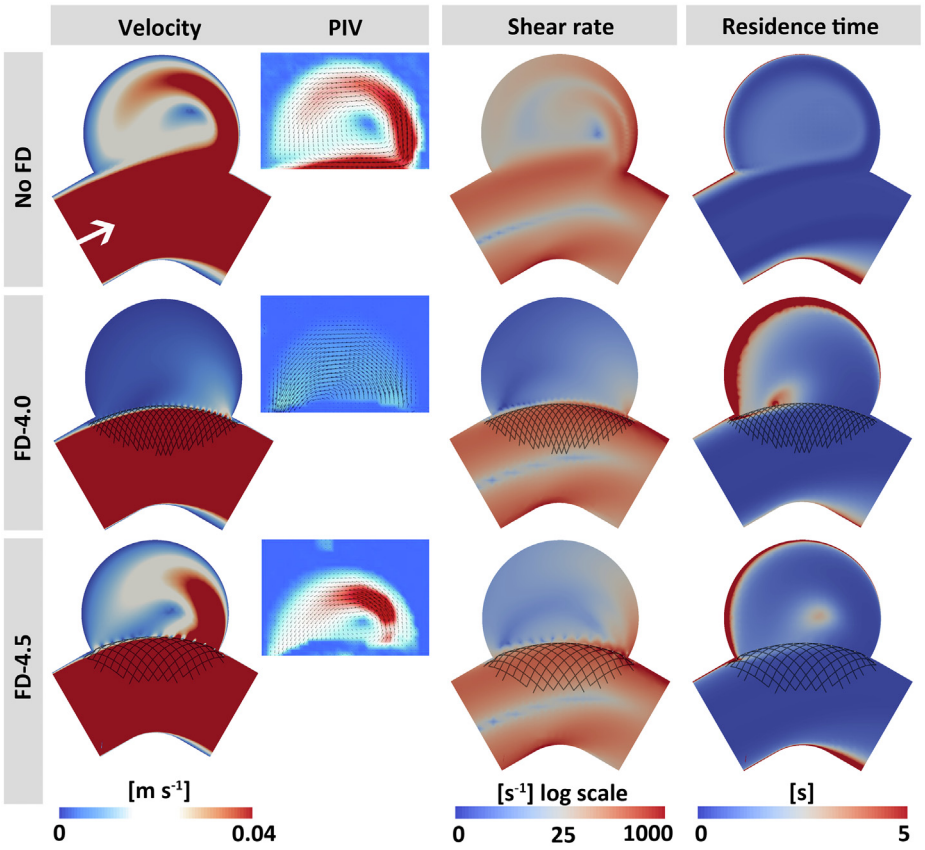

Fig. 3. Intra-aneurysmal haemodynamic quantification before and immediately after FD deployment. Velocity quantifications were made at the peak systole to enable comparisons with PIV measurements made in Gester et al. (2016). Flow direction is indicated with a white arrow in the top left panel and is the same in other panels.

3.2. Thrombus formation and comparison to in vitro observations

The thrombosis initiation criteria ($SR < 25\ s^{-1}$ and $RT > 5$ s) were not met in the simulations of intra-aneurysmal flow before FD placement, therefore, as expected, no clot formed in the aneurysm sac. According to previous studies (Anand et al., 2003, 2008), we assumed the clot to be formed in regions where the fibrin concentration is greater than 600 nM. In Fig. 4 (first row), the white iso-lines, drawn at fibrin concentrations of 600 nM, show the thrombus front. The dark red is associated with fibrin concentrations greater than 3500 nM, showing an almost complete conversion of plasma fibrinogen into fibrin. In agreement with (Gester et al., 2016), both FD's developed a clot that filled nearly the entire sac. In the FD-4.0 case, more pronounced formation and anchorage of fibrin strands to the proximal region of the FD were reported in the phantom experiments once the clot began to form. A proximal-to-distal direction of clot growth was reported in the FD-4.0 case, as opposed to no clear growth direction in the case treated with FD-4.5. Based on the transient results (see fibrin concentration contour plots at $t = 10$ s in Fig. 4), we observed that in the aneurysm treated with FD-4.0, the clot formed from the aneurysm proximal region and grew in a direction opposite to the entering flow jet direction to fill the aneurysm. In the aneurysm treated with FD-4.5, there was also a clot forming in the central part of the aneurysm (the central recirculation zone), growing with no preferred direction. We also observed a thicker band of high fibrin concentration started from the proximal region of FD and extended across the sac to the upper distal wall.

Fig. 4 (second row) shows contour plots of FiPi used to measure the effect of blood flow on the clot platelet content. In the FD-4.0 case, our results showed a platelet-rich clot ($FiPi > 0.15$) covering the entire aneurysm neck and extended towards the upper wall. However, in the FD-4.5 case, formation of the platelet-rich clot was limited to the central region of the sac. We observed a less platelet-rich clot at the proximal region of the aneurysm (in both cases) and in a small region at the centre of the platelet-rich clot formed in the centre of the aneurysm treated with the oversized FD. This observation agrees with the in vitro study (Gester et al., 2016), where a clot with a generally higher platelet content was reportedly induced by the FD-4.0, and regions with high platelet content around the central vortex were reported in the FD-4.5 case.

4. Discussion

4.1. Thrombus formation and model validation

The in vitro study (Gester et al., 2016) compared the effects of flow diversion by two stents in the same silicone phantom. In both cases, the phantom was filled with thrombus at the end of the experiment, at which point the authors removed the silicone model and provided snapshots of the induced clots. To enable comparisons with the in vitro experiments (Gester et al., 2016), we set a threshold on FiPi, the measure of platelet content, and extracted from this the platelet-rich clot morphology. The morphology of the clots obtained from our model showed the best qualitative agreement with snapshots of the phantom experiment, when we used $FiPi > 0.15$ as a threshold. Fig. 4, the third row, shows our model predictions of the morphology of the platelet-rich clot and snapshots of the phantoms taken from Gester et al. (2016). While we emphasise that $FiPi > 0.15$ is not a generalised threshold, we explored what happens to the morphology of the platelet-rich clots when we set a different threshold on FiPi. We examined thresholds $FiPi > 0.10$ and $FiPi > 0.20$. We used the Dice similarity coefficient

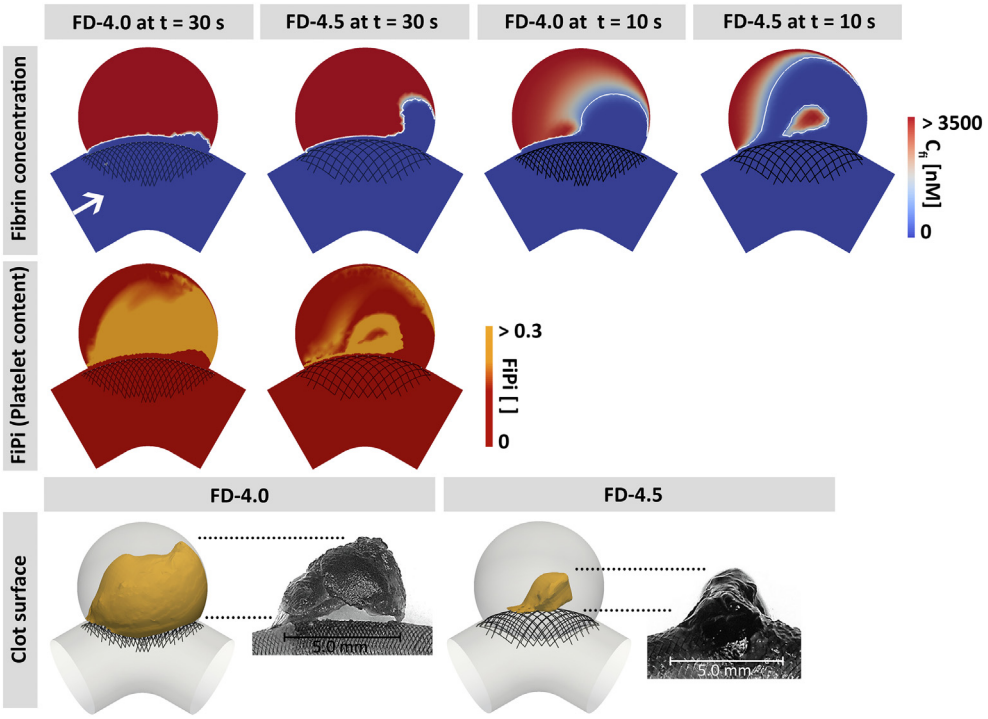

Fig. 4. Simulation of thrombosis in flow diverted aneurysms. In the first two rows, fibrin concentration contour plots are presented on the aneurysm sagittal mid-plane. In the first row, the white solid line represents a concentration of 600 nM. In the third row, for each flow-diverter, model predictions of the high-platelet content clot morphology (left) are compared against snapshots of the clots (right) from in vitro observations reported in Gester et al. (2016). The snapshots and the model predictions are presented in the same spatial scale and dotted lines are used to show the clot extent above the FDs. Flow direction is indicated with a white arrow in the top left panel and is the same in other panels.

(DSC) to compare the volumetric overlap between the morphologies produced by the new thresholds and the reference morphology extracted from FiPi > 0.15. High DSC scores 92.0% and 92.9% were achieved when the morphologies extracted from FiPi > 0.10 and FiPi > 0.20 thresholds was compared to the reference morphology, respectively. This demonstrates that thresholding FiPi is a robust way to predict.

Location of the clot and the growth direction. In both cases, in vitro experiments (Gester et al., 2016) showed that the clot started to form on the proximal wall. With FD-4.5, the course of thrombosis continued by formation of fibrin as a result of stagnation of blood at the centre sac, i.e., the central vortex. Fibrin then filled the aneurysm without a clear growth direction. With FD-4.0, the clot grew layer-by-layer and filled the aneurysm towards the distal wall. Our thrombosis model correctly predicted the locations of clot deposition and the growth directions reported in these in vitro experiments. Cebral et al. (2014) reported a layer-wise growth of clot from regions with smaller velocity, shear rates, and vorticity, i.e., the dome, towards the flow-diverted aneurysm neck. These results show that the thresholds we found based on residence time and shear rate were valid and that our model predicted realistic thrombi deposition location and growth direction.

Location of the high platelet content clot. In the FD-4.0 case, simulations indicated a transformation from inertia-driven to shear-driven flow (Fig. 3). Flow stasis along the proximal wall resulted in rapid formation of a less platelet-rich clot. However, during the course of thrombosis, the shear-driven, well-distributed blood flow promoted the attachment of platelets to the forming clot. This finally helped to form a homogeneous platelet-rich clot almost in the entire aneurysm. However in the aneurysm treated with the oversized stent FD-4.5, inertial effects persisted in the post-treatment flow and circulation in the aneurysm sac was observed (Fig. 3). Although less pronounced than in the FD-4.0, extensive stasis along the proximal wall resulted in the rapid formation of a less platelet-rich clot. We also observed the formation of a clot in the central vortex. In contrast to FD-4.0, the inertia-driven flow jet was not slow enough to promote platelet attachment. This flow pattern resulted in a heterogeneous clot with a higher platelet concentration limited to the outer layers of clot initially formed in the central vortex (Fig. 4). These findings agreed qualitatively with the experimental observations in Gester et al. (2016) and provided support to the hypothesis that rapid formation of clot in regions of extensive stasis results in a less platelet-rich clot, however, as the clot grows and interacts with the blood flow, more platelets come in contact with the forming clot, which results in formation of a more platelet-rich clot (Kulcsár et al., 2011; Xiang et al., 2014).

Coverage of the aneurysm neck. Formation of a platelet-rich organised clot over the aneurysm neck is essential to close the aneurysm and facilitate endothelialisation (Kadirvel et al., 2014; Szikora et al., 2015). In our simulations, we did not consider surface reactions on the FD struts. However, in the FD-4.5, we observed the formation of a thin platelet-rich layer covering the proximal section of the aneurysm neck and extending to a thicker layer in the central section of the neck. The distal section of the neck remained patent. In the FD-4.0, we observed a thick platelet-rich layer covering the aneurysm neck. Similar behaviour was reported in in vitro experiments (Gester et al., 2016) and also in Kadirvel et al. (2014),Szikora et al. (2015), where the FD failed to close the sac in real aneurysms. In the FD-4.5, the clot formed in the central region of the sac was surrounded by a flow jet that prevented a full coverage of the neck with a stable clot. The FD-4.0 altered the flow pattern inside the sac and facilitated layer-wise growth of the clot and finally the full coverage of the aneurysm neck with a platelet-rich clot.

4.2. Clinical utility

Treatment planning of flow diversion is usually based on the morphology of the aneurysm (Becske et al., 2013; Fischer et al.,

2012). Aside from symptomatic aneurysms, large and giant aneurysms and those with a high aspect ratio or complex morphology are thought to be prone to post-FD haemorrhage (Kulcsár et al., 2011). Immediately after deployment, the efficacy of the FD is evaluated by measuring the reduction of flow into the aneurysmal sac by angiographic examination. However, post-operative rupture was reported in several cases with excellent immediate angiographic results after FD deployment (Kulcsár et al., 2011; Kuzmik et al., 2013; Turowski et al., 2011).

CFD-modellers have suggested different haemodynamic criteria for predicting successful occlusion of aneurysms after flow diversion. For example, Ouared et al. (2016) reported a minimum reduction of 35% in the aneurysm mean velocity after flow diversion as a criterion for predicting successful occlusion. Mut et al. (2015) reported post-treatment velocity and shear rate of 1.31 cm/s and 16.35 s^{-1}, respectively, as criteria for successful aneurysm occlusion. In our simulations, post-treatment haemodynamics in both FD-4.0 and FD-4.5 cases met the success criteria suggested in the above studies. However, the two cases developed a clot with different qualities. This shows that purely haemodynamic assessments cannot predict the likelihood of formation of a stable clot. To comprehensively assess post-FD occlusion, it is necessary to consider the potential quality of the FD-induced clot, i.e., whether flow diversion results in a stable white clot or a red unorganised clot. Our model showed promise in predicting the biochemical composition of clot structural components, fibrin and platelets, and thus, the likelihood of formation of a fibrin and platelet-rich white thrombi after flow diversion.

Also there is evidence that in aneurysm treatment with FD, formation of a stable white clot over the aneurysm neck and the consequent formation of neo-intimal layer and FD endothelialisation are of superior importance than FD-induction of the thrombi inside the aneurysm body (Kadirvel et al., 2014; Szikora et al., 2015). Cebral et al. (2014) trained a statistical model to predict the local occlusion based on local haemodynamics and found poorer predictions near the aneurysm neck, when compared to other regions of the flow diverted aneurysm. This magnifies the utility of models similar to the one in the present work to further improve personalised assessment of aneurysm flow diversion.

4.3. Limitations

Low-shear stagnant flow is believed to be the main driver of thrombosis in flow-diverted aneurysms (Ouared et al., 2016; Rayz et al., 2010). Dual anti-platelet inhibition regimens are prescribed to minimise, but not eliminate, mechanical high-shear induced platelet activation in aneurysms treated with FDs (Heller et al., 2013). In our experiments, we observed blood flow passing through the FD struts to have a maximum shear rate of about 1000 s^{-1} which was below the shear rate level to activate the platelets (3000 s^{-1}Roth, 1991). Maximum shear stress near the struts was less than 15 Pa in our simulations. According to the Hellums locus of high shear-induced platelet activation (Hellums, 1994), such shear stress level requires an exposure time greater than 100 s to activate platelets. Given the near-strut maximum residence time in our simulations, about 1 s, mechanical activation does not likely to play a significant role in our experiments. Although we did not explicitly model mechanical activation, we analysed the sensitivity of our results to the background platelet activation level. In this way, we were able to implicitly measure the effect of putative mechanically activated platelets being washed into the aneurysm sac. The reference background platelet activation was 5% in our experiments. For the FD-4.0 case, we repeated our experiments with 1% and 10% activation levels, maintaining the concentration of the resting platelets. Changing the background activation level did not affect the growth pattern and the locations of low/high platelet content clot formation and deposition. We also performed a point-wise comparison between FiPi values throughout the sac. FiPi values were 4 ± 11% lower when using 1% background platelet activation and 7 ± 18% higher when 10% background activation level was used. We then studied the sensitivity of the platelet-rich clot morphology to the background platelet activation level. We set FiPi > 0.15 as a threshold and extracted the platelet-rich clot morphology. High DSC scores 95.5% and 94.0% were achieved when the reference clot morphology (based on 5% background activation) was compared with morphologies obtained from simulations with 1% and 10% background platelet activation levels, respectively.

The thrombosis model parameters were taken from experimental literature or relevant computational studies that performed sensitivity analyses, except the fibrin concentration at which rate of platelet attachment to the fibrin mesh is half of its maximum value, $C_{fi,50}$. A fixed value of this concentration was used in all our simulations. A sensitivity analysis was performed with twice and half of the original concentration, i.e., $C_{fi,50} = 60$ nM. We observed only small effects on the location and extent of the thrombus deposition, and on the distribution of platelets in the final clot. DSC scores of 89.2% and 92.5% were achieved when the platelet-rich clot morphology obtained with $C_{fi,50} = 60$ nM was compared to morphologies obtained with two times and half of this value, respectively. More comprehensive analyses must determine the sensitivity of clot composition and morphology to the model parameters.

Due to the computational burden required, the time scale of our thrombosis model is not representative of the physiological time scale of FD-induced clot formation and aneurysm occlusion, i.e., weeks to months. We relate this to: (i) the extensive simplification of the thrombosis chemical network, neglecting several molecular and cellular level phenomena involved in initiation, progression, and inhibition of thrombosis course after flow diversion, (ii) neglecting phenomena like lysis, organisation, and contraction of the clot (iii) neglecting the effect of flow pulsation on the reactions, especially on the initiation reactions when the clot-related concentrations are small, and (iv) the effect of anti-coagulants and anti-platelets that are both common in flow diversion patients. We did not consider such anticoagulation in our model.

Augsburger et al. (2009) showed that flow pulsation is not a major determinant of FD performance in terms of reducing aneurysmal velocity. Since we were mostly interested in the final state of the clot and not in phenomena like thrombus breakdown, we did not consider flow pulsatility and our simulations were performed using a non-pulsatile (steady) inflow boundary condition, however, the thrombosis model can easily be run with pulsatile boundary conditions.

5. Conclusion

The thrombosis model in the present study was developed to predict the platelet content distribution in intra-aneurysmal clots formed after flow diversion. The predictions made by the model showed qualitative similarities in the clotting pattern and platelet composition when compared with an in vitro phantom experiment performed by an independent research group in Gester et al. (2016). We also compared our model predictions against the literature on qualitative thrombotic behaviour in aneurysms treated with flow diverters.

Declaration of Competing Interest

All the authors declare no conflicts of interest exist.

Acknowledgements

A. Sarrami-Foroushani, T. Lassila, and A.F. Frangi were funded by the H2020 Programme project InSilc *"In-silico trials for drug-eluting BVS design, development and evaluation"* (H2020-SC1-2017-CNECT-2-777119). T. Lassila and A.F. Frangi were funded by the 7th Framework Programme project VPH-DARE@IT *"Virtual Physiological Human: DementiA Research Enabled by IT"* (FP7-ICT-2011-5.2-601055). A.F. Frangi acknowledges support from the Royal Academy of Engineering under the RAEng Chairs in Emerging Technologies scheme (CiET1919/19).

Appendix A. Supplementary material

Supplementary data associated with this article can be found, in the online version, at https://doi.org/10.1016/j.jbiomech.2019.04.045.

References

Aida, Y., Shimano, K., 2013. Modelling of blood coagulation in cerebral aneurysms. WIT Trans. Biomed. Health 17, 51–62.
Anand, M., Rajagopal, K., Rajagopal, K., 2003. A model incorporating some of the mechanical and biochemical factors underlying clot formation and dissolution in flowing blood. Comput. Math. Methods Med. 5 (3–4), 183–218.
Anand, M., Rajagopal, K., Rajagopal, K., 2008. A model for the formation, growth, and lysis of clots in quiescent plasma. A comparison between the effects of antithrombin III deficiency and protein C deficiency. J. Theor. Biol. 253 (4), 725–738.
Augsburger, L., Farhat, M., Reymond, P., Fonck, E., Kulcsar, Z., Stergiopulos, N., Rüfenacht, D., 2009. Effect of flow diverter porosity on intraaneurysmal blood flow. Clin. Neuroradiol. 19 (3), 204–214.
Becske, T., Kallmes, D., Saatci, I., McDougall, C., Szikora, I., Lanzino, G., Moran, C., Woo, H., Lopes, D., Berez, A., et al., 2013. Pipeline for uncoilable or failed aneurysms: results from a multicenter clinical trial. Radiology 267 (3), 858–868.
Bodnár, T., Fasano, A., Sequeira, A., 2014. Mathematical models for blood coagulation. In: Fluid-Structure Interaction and Biomedical Applications. Springer, pp. 483–569.
Byrne, J., Szikora, I., 2012. Flow diverters in the management of intracranial aneurysms: a review. EJMINT Original Article. 1225000057:29.
Cebral, J., Mut, F., Raschi, M., Hodis, S., Ding, Y.-H., Erickson, B., Kadirvel, R., Kallmes, D., 2014. Analysis of hemodynamics and aneurysm occlusion after flow-diverting treatment in rabbit models. Am. J. Neuroradiol. 35 (8), 1567–1573.
Chow, M., McDougall, C., O'Kelly, C., Ashforth, R., Johnson, E., Fiorella, D., 2012. Delayed spontaneous rupture of a posterior inferior cerebellar artery aneurysm following treatment with flow diversion: a clinicopathologic study. Am. J. Neuroradiol. 33 (4), E46–E51.
de Sousa, D., Vallecilla, C., Chodzynski, K., Jerez, R., Malaspinas, O., Eker, O., Ouared, R., Vanhamme, L., Legrand, A., Chopard, B., et al., 2015. Determination of a shear rate threshold for thrombus formation in intracranial aneurysms. J. Neurointervent. Surg. 8, 853–858.
Fischer, S., Vajda, Z., Perez, M., Schmid, E., Hopf, N., Bäzner, H., Henkes, H., 2012. Pipeline embolization device (PED) for neurovascular reconstruction: initial experience in the treatment of 101 intracranial aneurysms and dissections. Neuroradiology 54 (4), 369–382.
Gester, K., Lüchtefeld, I., Büsen, M., Sonntag, S., Linde, T., Steinseifer, U., Cattaneo, G., 2016. In vitro evaluation of intra-aneurysmal, flow-diverter-induced thrombus formation: a feasibility study. Am. J. Neuroradiol. 37 (3), 490–496.
Girdhar, G., Andersen, A., Pangerl, E., Jahanbekam, R., Ubl, S., Nguyen, K., Wainwright, J., Wolf, M.F., 2018. Thrombogenicity assessment of Pipeline Flex, Pipeline Shield, and FRED flow diverters in an in vitro human blood physiological flow loop model. J. Biomed. Mater. Res. A 106 (12), 3195–3202.
Girdhar, G., Ubl, S., Jahanbekam, R., Thinamany, S., Belu, A., Wainwright, J., Wolf, M. F., 2019. Thrombogenicity assessment of Pipeline, Pipeline Shield, Derivo and P64 flow diverters in an in vitro pulsatile flow human blood loop model. eNeurologicalSci 14, 77–84.
Heller, R.S., Dandamudi, V., Lanfranchi, M., Malek, A.M., 2013. Effect of antiplatelet therapy on thromboembolism after flow diversion with the Pipeline embolization device. J. Neurosurg. 119 (6), 1603–1610.
Hellums, J.D., 1994. 1993 Whitaker lecture: biorheology in thrombosis research. Ann. Biomed. Eng. 22 (5), 445–455.
Kadirvel, R., Ding, Y.-H., Dai, D., Rezek, I., Lewis, D., Kallmes, D., 2014. Cellular mechanisms of aneurysm occlusion after treatment with a flow diverter. Radiology 270 (2), 394–399.
Kuharsky, A., Fogelson, A., 2001. Surface-mediated control of blood coagulation: the role of binding site densities and platelet deposition. Biophys. J. 80 (3), 1050–1074.
Kulcsár, Z., Szikora, I., 2012. The ESMINT retrospective analysis of delayed aneurysm ruptures after flow diversion (RADAR) study. EJMINT Original Article 2012, 1244000088.
Kulcsár, Z., Houdart, E., Bonafe, A., Parker, G., Millar, J., Goddard, A., Renowden, S., Gal, G., Turowski, B., Mitchell, K., et al., 2011. Intra-aneurysmal thrombosis as a possible cause of delayed aneurysm rupture after flow-diversion treatment. Am. J. Neuroradiol. 32 (1), 20–25.
Kuzmik, G., Williamson, T., Ediriwickrema, A., Andeejani, A., Bulsara, K., 2013. Flow diverters and a tale of two aneurysms. J. Neurointerv. Surg. 5 (4), e23.
Martínez-Galdámez, M., Lamin, S.M., Lagios, K.G., Liebig, T., Ciceri, E.F., Chapot, R., Stockx, L., Chavda, S., Kabbasch, C., Farago, G., et al., 2017. Periprocedural outcomes and early safety with the use of the Pipeline Flex Embolization Device with Shield Technology for unruptured intracranial aneurysms: preliminary results from a prospective clinical study. J. Neurointerv. Surg. 9 (8), 772–776.
Mut, F., Raschi, M., Scrivano, E., Bleise, C., Chudyk, J., Ceratto, R., Lylyk, P., Cebral, J., 2015. Association between hemodynamic conditions and occlusion times after flow diversion in cerebral aneurysms. J. Neurointerv. Surg. 7 (4), 286–290.
Nesbitt, W., Westein, E., Tovar-Lopez, F., Tolouei, E., Mitchell, A., Fu, J., Carberry, J., Fouras, A., Jackson, S., 2009. A shear gradient–dependent platelet aggregation mechanism drives thrombus formation. Nat. Med. 15 (6), 665.
Ngoepe, M., Ventikos, Y., 2016. Computational modelling of clot development in patient-specific cerebral aneurysm cases. J. Thromb. Haemostasis 14 (2), 262–272.
Ouared, R., Chopard, B., Stahl, B., Rüfenacht, D., Yilmaz, H., Courbebaisse, G., 2008. Thrombosis modeling in intracranial aneurysms: a lattice boltzmann numerical algorithm. Comput. Phys. Commun. 179 (1–3), 128–131.
Ouared, R., Larrabide, I., Brina, O., Bouillot, P., Erceg, G., Yilmaz, H., Lovblad, K.-O., Pereira, V., 2016. Computational fluid dynamics analysis of flow reduction induced by flow-diverting stents in intracranial aneurysms: a patient-unspecific hemodynamics change perspective. J. Neurointerv. Surg., pages neurintsurg–2015
Ou, C., Huang, W., Yuen, M.-F., 2017. A computational model based on fibrin accumulation for the prediction of stasis thrombosis following flow-diverting treatment in cerebral aneurysms. Med. Biol. Eng. 55 (1), 89–99.
Park, M.S., Taussky, P., Albuquerque, F.C., 2017. Flow Diversion of Cerebral Aneurysms. Thieme.
Rayz, V., Boussel, L., Ge, L., Leach, J., Martin, A., Lawton, M., McCulloch, C., Saloner, D., 2010. Flow residence time and regions of intraluminal thrombus deposition in intracranial aneurysms. Ann. Biomed. Eng. 38 (10), 3058–3069.
Roth, G.J., 1991. Developing relationships: arterial platelet adhesion, glycoprotein ib, and leucine-rich glycoproteins. Blood 77 (1), 5–19.
Shimano, K., Aida, Y., Nakagawa, Y., 2010. Slowness of blood flow and resultant thrombus formation in cerebral aneurysms. J. Biorheol. 24 (2), 47.
Szikora, I., Turányi, E., Marosfoi, M., 2015. Evolution of flow-diverter endothelialization and thrombus organization in giant fusiform aneurysms after flow diversion: a histopathologic study. Am. J. Neuroradiol. 36 (9), 1716–1720.
Tan, K.T., Lip, G.Y., 2003. Red vs white thrombi: treating the right clot is crucial. Arch. Inern. Med. 163 (20), 2534–2535.
Taylor, L.I., Dickerson, J.C., Dambrino, R.J., Kalani, M.Y.S., Taussky, P., Washington, C. W., Park, M.S., 2017. Platelet testing in flow diversion: a review of the evidence. Neurosurg. Focus 42 (6), E5.
Turowski, B., Macht, S., Kulcsár, Z., Hänggi, D., Stummer, W., 2011. Early fatal hemorrhage after endovascular cerebral aneurysm treatment with a flow diverter (SILK-stent). Neuroradiology 53 (1), 37–41.
Undas, A., Ariëns, R., 2011. Fibrin clot structure and function: a role in the pathophysiology of arterial and venous thromboembolic diseases. Arterioscler. Thromb. Vasc. Biol. 31 (12), e88–e99.
Versteeg, H., Heemskerk, J., Levi, M., Reitsma, P., 2013. New fundamentals in hemostasis. Physiol. Rev. 93 (1), 327–358.
Weisel, J., Litvinov, R., 2008. The biochemical and physical process of fibrinolysis and effects of clot structure and stability on the lysis rate. Cardiovasc. Hematol. Agents Med. Chem. 6 (3), 161–180.
Wolberg, A.S., Aleman, M.M., Leiderman, K., Machlus, K.R., 2012. Procoagulant activity in hemostasis and thrombosis: Virchow's triad revisited. Anesth. Analg. 114 (2), 275.
Xiang, J., Ma, D., Snyder, K., Levy, E., Siddiqui, A., Meng, H., 2014. Increasing flow diversion for cerebral aneurysm treatment using a single flow diverter. Neurosurg. 75 (3), 286–294.